Supporting Information

Coplanar Indoline-Functionalized Fullerene with Elevated LUMO for Tin Halide Perovskite Photovoltaics

Pengyu Yan,[a] Tianqi Ma,[a] Wanqi Jin,[a] Jie Luo,[a] Huanhuan Yao,[a] Xilong Yang,[a] Hanyu Zhang,[a] Liming Ding,[b] and Feng Hao*[a]

[a] *School of Materials and Energy, University of Electronic Science and Technology of China, Chengdu 611731, China.*
[b]*School of Chemical Engineering and Light Industry, Guangdong University of Technology, Guangzhou 510006, China*

*Corresponding author, E-mail: haofeng@uestc.edu.cn;

1. Materials

N, N-dimethylformamide (DMF) (99.8%, Sigma-Aldrich), dimethyl sulfoxide (DMSO)

(99.9%, Sigma-Aldrich), chlorobenzene (CB) (99.8%, Sigma-Aldrich), isopropanol (IPA) (99.5%, Sigma-Aldrich), *o*-dichlorobenzene (*o*-DCB) (99.0%, Admas-beta), dichloromethane (DCM) (99.5%, Admas-beta), petroleum ether (PE) (60–90 °C, 99.0%, Admas-beta), and toluene (99.5%, Admas-beta). All solvents were used as received without further purification.

Formamidinium iodide (FAI) (99.99%, GreatCell), methylammonium bromide (MABr) (99.9%, GreatCell), 2-phenylethanamine iodide (PEAI) (99.5%, GreatCell), tin powder (99.8%, Admas-beta), tin fluoride (SnF_2) (99%, Admas-beta), tin (II) iodide (SnI_2) (99.99%, 3A), poly (3,4-ethylene dioxythiophene)-poly (styrene sulfonate) (PEDOT: PSS) (Mn=15,000-25,000, Xi'an Yuri Solar Co. Ltd), bathocuproine (BCP) (98.0%, Admas-beta), fullerene C_{60} (99.9%, Admas-beta), 5-methoxy-2,3-dihydro-indoline (96.0%, Admas-beta), 4-bromobenzaldehyde (99.0%, Admas-beta), cesium carbonate (Cs_2CO_3) (99.0%, Admas-beta), tris(dibenzylideneacetone)dipalladium $Pd_2(dba)_3$, (99.0%, Admas-beta), 1.1'-binaphthyl-2.2'-diphemyl phosphine (BINAP), (98%, Admas-beta). Unless otherwise noted, all chemicals were used in their as-received state.

2. Device fabrication

ITO glass substrates were sequentially cleaned with deionized water, ethanol, acetone, and isopropanol, followed by thorough drying under a nitrogen stream. The cleaned ITO substrates were then treated in a UV-ozone chamber for 15 min. A 90 μL aliquot of PEDOT:PSS aqueous solution was deposited onto the ITO surface and spin-coated at 4000 rpm for 50 s, followed by thermal annealing at 140 °C for 20 min. For the perovskite precursor solution, 128.98 mg of formamidinium iodide (FAI), 27.99 mg of methylammonium bromide (MABr), 372.52 mg of tin iodide (SnI_2), 15.67 mg of tin fluoride (SnF_2), and 4 mg of Sn powder were dissolved in 1 mL of a mixed solvent of

DMSO: DMF (1:4, v/v). The perovskite precursor solution, after being stirred for 12 h, was spin-coated onto the substrate at 8000 rpm for 60 s. At the 12th second of spinning, 150 μL of chlorobenzene antisolvent was dispensed onto the film. The film was then annealed for 10 min at 80 ℃. Next, 55 μL F6 and F6-IND solution (20 mg mL^{-1} in CB) was spin-coated at 2000 rpm for 50 s and annealed at 70 °C for 8 min. This was followed by deposition of a bathocuproine (BCP) layer from a 0.8 mg mL^{-1} isopropanol (IPA) solution, spin-coated at 6000 rpm for 30 s and annealed at 70 °C for 10 min. Finally, a silver (Ag) electrode (~100 nm thick) was thermally evaporated under high vacuum.

3. Characterization

3.1 Materials Characterization

^{1}H NMR and ^{13}C NMR spectra were recorded on Bruker AVANCE III in solution at 400 MHz. Proton (^{1}H) NMR information is described in the following format: multiplicities (s = singlet, d = doublet, t = triplet, m = multiplet, br = broad), coupling constants (*J*) in Hertz (Hz), the number of protons. Proton (^{13}C) NMR spectra are reported in ppm (δ) relative to residual $CDCl_3$. Matrix-assisted laser desorption/ionization time-of-flight mass spectrometry (MALDI-TOF MS) was performed on a Bruker Autoflex Speed instrument. The UV-Vis data were obtained by using UV-2600 (Shimadzu). The steady PL and time-resolved PL spectra were performed using PTI QuantaMaster 8000. The excitation source of PL spectra was a mono-chromatized Xe lamp (450W) with a 405 nm pulsed laser.

3.2 Device Characterization

J-V curves were characteristics were measured by solar simulator (San-EI Electric) under simulated AM1.5G (100 mW cm^{-2}) illumination and Keithley 2400 source. The light intensity was calibrated by a standard silicon solar cell. EQE data were measured by using QE-R (Enli tech, Taiwan). The dark J-V, Mott-Schottky (M-S), electronic impedance spectroscopy (EIS). Transient photovoltage (TPV) decay and Photo-CELIV data were obtained by Piaos 4.0 system (FLUXiM).

Note 1. Cyclic voltammetry (CV)[1–3]

Cyclic voltammetry (CV) experiment was performed with a 760E electrochemical workstation constructed by a Pt disk as the working electrode, a Pt wire as the counter electrode and Ag/AgCl as the reference electrode. The CV scans of the electron transport materials (F6 and F6-IND) were performed in an *o*-dichlorobenzene (*o*-DCB)/acetonitrile (CH_3CN) mixed solvent (5:1, v/v) containing 0.1 M tetrabutylammonium hexafluorophosphate (n-Bu_4NPF_6) as the supporting electrolyte, at a scan rate of 100 mV s^{-1} . Ferrocene (Fc/Fc^+) was used as an internal standard, with its redox potential referenced to the vacuum level at -4.80 eV. The LUMO energy levels were estimated from the onset of the reduction potential ($E_{red,onset}$) according to the following equation:

$$E_{LUMO} = -[E_{red}^{onest} + 4.8\ ]$$

Where E_{red}^{onset} is the onset of reduction potential *vs.* Fc/Fc^+

Note 2. Equation of bi-exponential decays for TRPL[4]

TRPL was fitting by a bi-exponential decay as the following equation.

$$Y = A_1 e^{\left(-\frac{t}{\tau_1}\right)} + A_2 e^{\left(-\frac{t}{\tau_2}\right)}$$

$$\tau_{avg=} \frac{\sum A_i \tau_i}{\sum A_i}$$

Where τ_1 is the charge extraction and transport, τ_2 are the trap assisted non-radiative recombination particularly at interfaces/grain boundaries.

Note 3. Theoretical calculation[5]

Density functional theory (DFT) calculations were carried out using the Gaussian 16 program at the B3LYP/6-31G(d) level to optimize the ground-state geometries of F6 and F6-IND in the gas phase. The resulting wavefunction files (.fch) were subsequently analyzed with Multiwfn (version 3.8) to extract detailed electronic structure information. Specifically, the projected density of states (PDOS) was obtained by projecting the Kohn–Sham molecular orbitals onto individual atomic orbitals; Hirshfeld

atomic charges were computed based on electron density partitioning; and the localized orbital locator (LOL) iso-surfaces were generated to visualize regions of high electron localization and covalent bonding character.

4. Synthetic procedures

The synthetic routes of F6-IND is illustrated in Scheme 1. F6 was synthesized according to previous report.[6] Fullerene C_{60}, 5-methoxy-2,3-dihydro-indoline (5-MeO-IND), 4-bromobenzaldehyde (4-BrBzH) was purchase from Admas-beta.

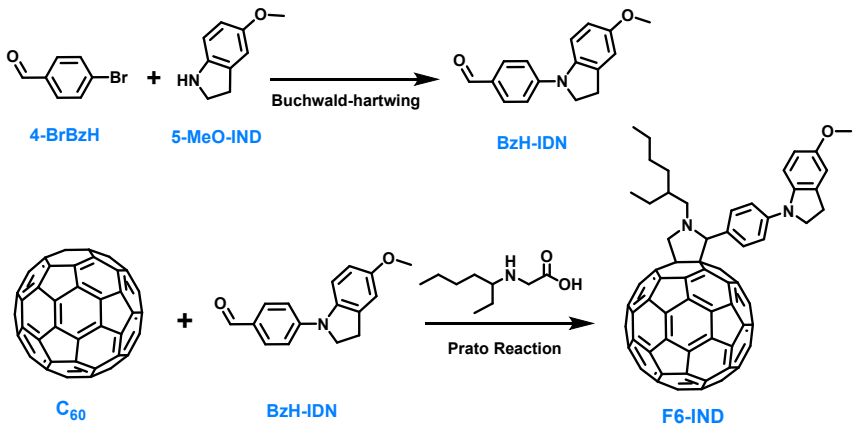

Scheme 1 Synthesis route of F6-IND.

(1) Synthesis of BzH-IND

A mixture of 4-BrBzH (370.04 mg, 2.0 mmol), 5-MeO-IND (358.06 mg, 2.4 mmol), Cs_2CO_3 (977.46 mg, 3.0 mmol), $Pd_2(dba)_3$ (91.57 mg, 5%), and 1.1'-Binaphthyl-2.2'-diphemyl phosphine (BINAP) (124.53 mg, 10%) are dissolved in 20 ml toluene and refluxed under argon overnight. After cooling down, the reaction mixture was filtered to remove insoluble material. After removal of the solvent, the crude product is purified by silica gel column chromatography with petroleum ether/ethyl acetate (5/1, v/v) as the eluent to afford BzH-IND as a deep red liquid. (320 mg, 63.7%) ^{1}H NMR (400 MHz, $CDCl_3$, ppm) δ: 9.80 (s, 1H, CHO), 7.81 (d, 2H, J= 5.6 Hz, ArH),7.27 (s, 1H, ArH), 7.21 (d, 2H, J= 5.6 Hz, ArH), 6.83 (s, 1H, ArH), 6.70 (d, 1H, J= 5.6 Hz, ArH), 4.05 (t, 2H, J= 5.6 Hz, CH_2), 3.79 (s, 3H, CH_3), 3.17 (t, 2H, J= 5.2 Hz, CH_2)

(2) Synthesis of F6-IND

C_{60} (360. mg, 0.5 mmol) and N-(2-Ethylhexyl) glycine (187.2 mg, 1.0 mmol) was added to a solution of BzH-IND (158.9 mg, 0.6 mmol) in *o*-DCB (10 ml) under argon. After stirring at 120 °C for 8 h, the reaction mixture was purified by flash column chromatography on silica gel using petroleum ether/dichloromethane (1:1, v/v) as the eluent. After condensing, the organic layer was precipitated into methanol (200 ml). The crude product was then collected by filtration. Then, the solid is recrystallized from a carbon disulfide and methanol mixture to afford a dull brown solid (122 mg, 22.1%). ^{1}H NMR (400MHz, $CDCl_3$, ppm) δ: 7.73 (br s, 2H, ArH), 7.20 (d, 2H, J=8.0 Hz, ArH), 7.11 (d, 1H, J=10.4 Hz, ArH), 6.79 (s, 1H, ArH), 6.63 (d, 2H, J=11.2 Hz, ArH), 5.09 (d, 1H, J=10.4 Hz, CH_2), 4.99 (s, 1H, CH), 4.06 (d, 1H, J=9.2 Hz, CH_2), 3.97 (t, 2H, J=10.8 Hz, CH_2), 3.76 (s, 3H, CH_3), 3.11-3.00 (m, 3H), 2.50 (t, 1H, J=9.6 Hz), 1.99 (br s, 1H, CH_2), 1.76-1.71 (m, 1H, CH), 1.50-1.35 (m, 6H, CH_2), 1.10-0.94 (m, 6H, CH_3). ^{13}C NMR (150MHz, $CDCl_3$, ppm) δ: 157.0, 154.5, 154.2, 154.0, 153.4, 147.4, 147.1, 146.7, 146.6, 146.4, 146.3, 146.2, 146.0, 145.9, 145.7, 145.6, 145.5, 145.4, 145.2, 144.8, 144.5, 143.2, 143.1, 142.8, 142.6, 142.5, 142.4, 142.2, 142.1, 141.9, 141.7, 141.6, 140.5, 140.2, 140.0, 139.6, 112.4, 111.3, 109.0, 82.8, 69.1, 67.3, 57.6, 56.0, 52.1, 38.5, 31.9, 31.4, 29.7, 28.5, 25.6, 24.4, 23.6, 23.3, 22.8, 14.6, 14.4, 12.0, 10.6. HR-TOF-MS (MALDI) *m/z:* $[M+H]^+$ calcd. for $C_{85}H_{35}N_2O$, 1100.2285; found, 1100.3641.

5. Supplementary figures and tables

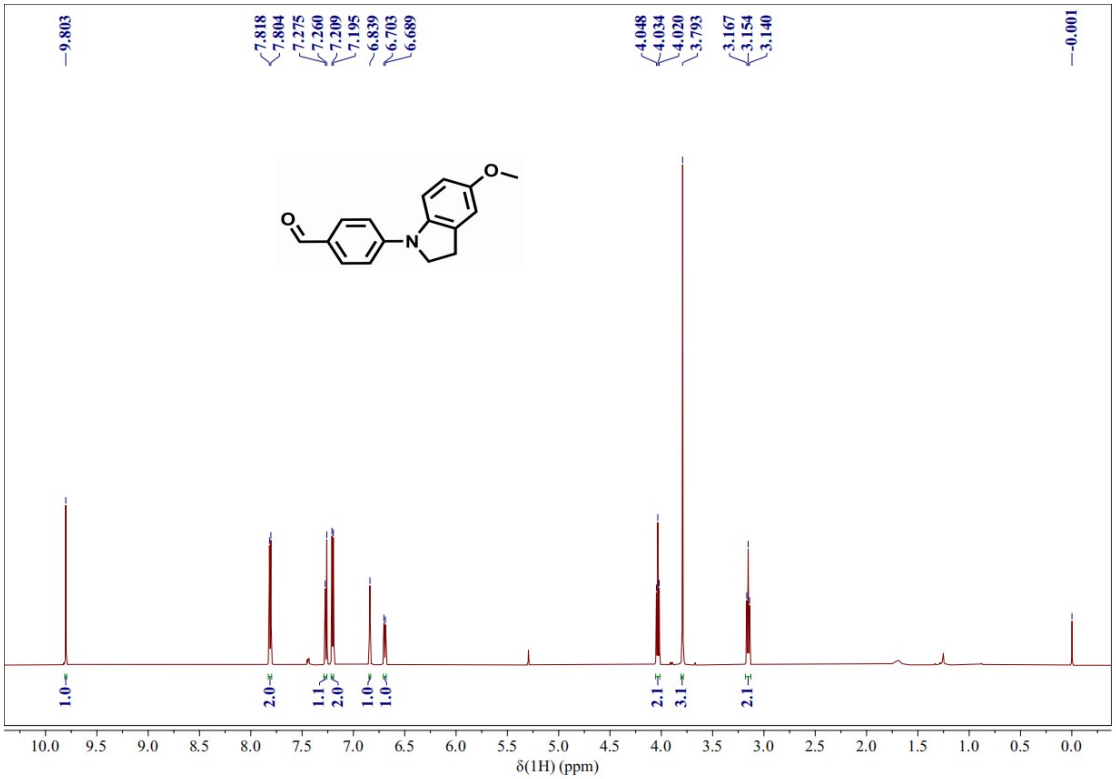

Figure S1. ^{1}H NMR spectrum of BzH-IND in $CDCl_3$.

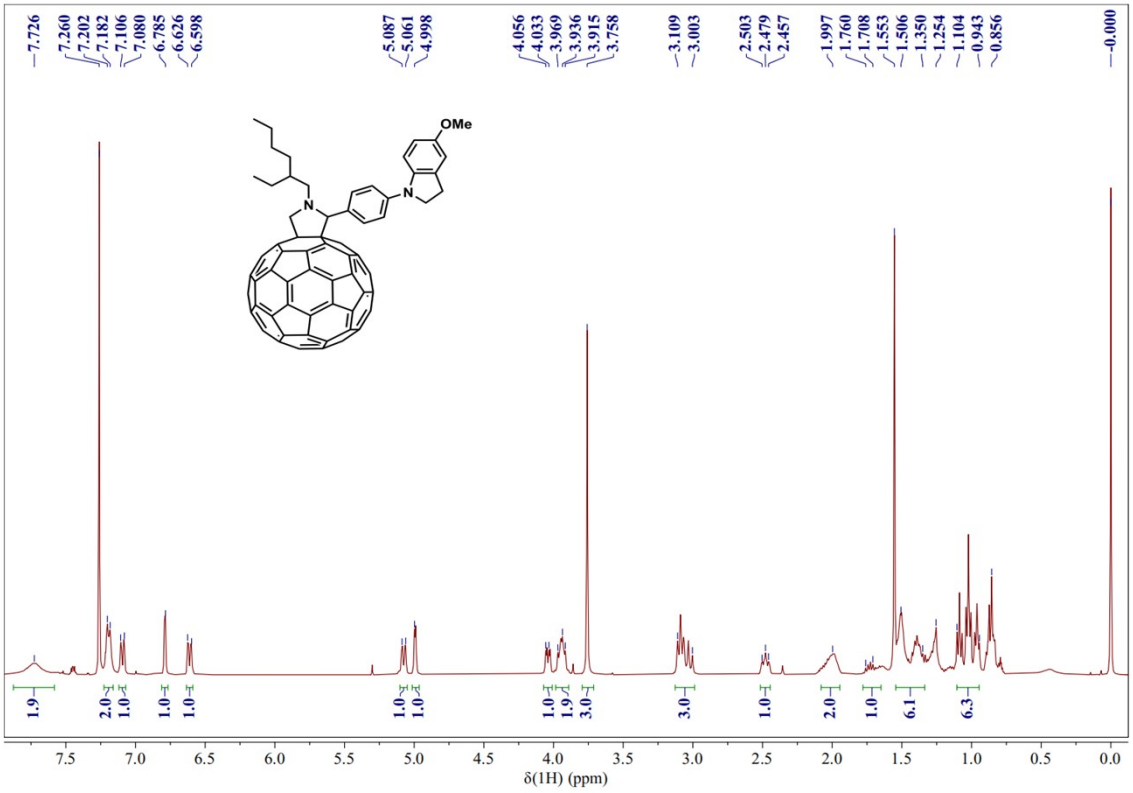

Figure S2. ^{1}H NMR spectrum of F6-IND in $CDCl_3$.

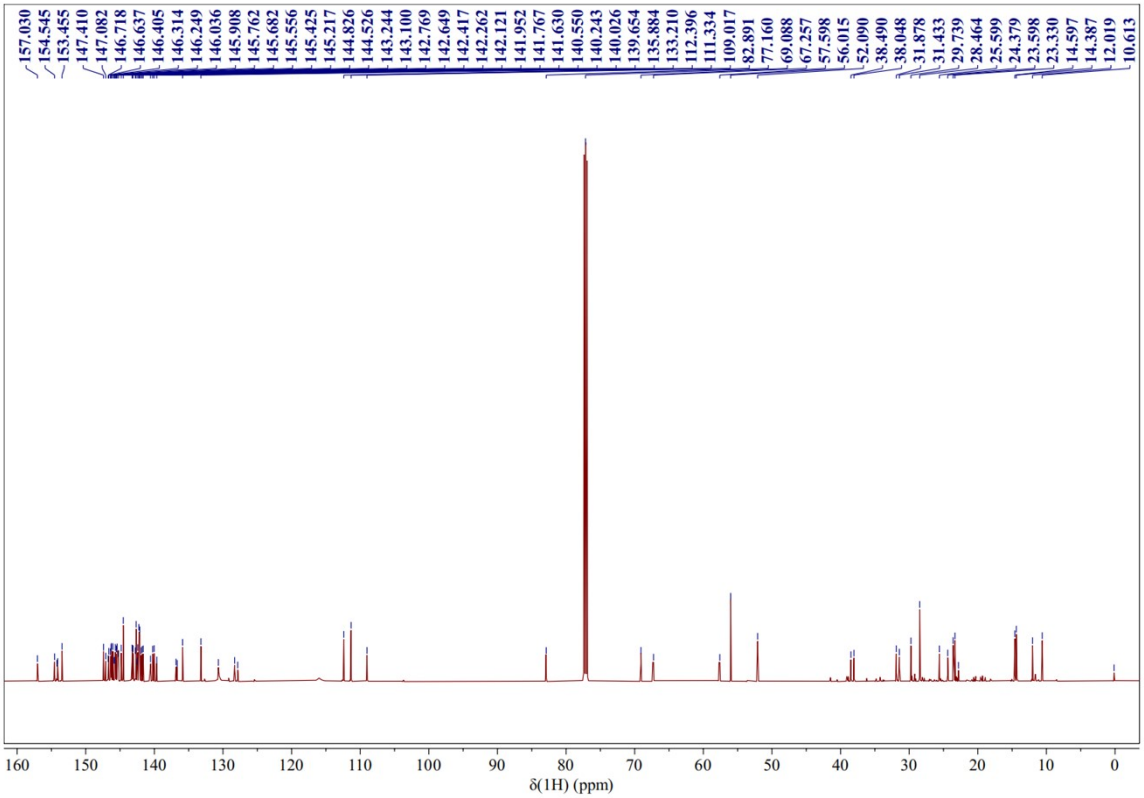

Figure S3. ^{13}C NMR spectrum of F6-IND in $CDCl_3$.

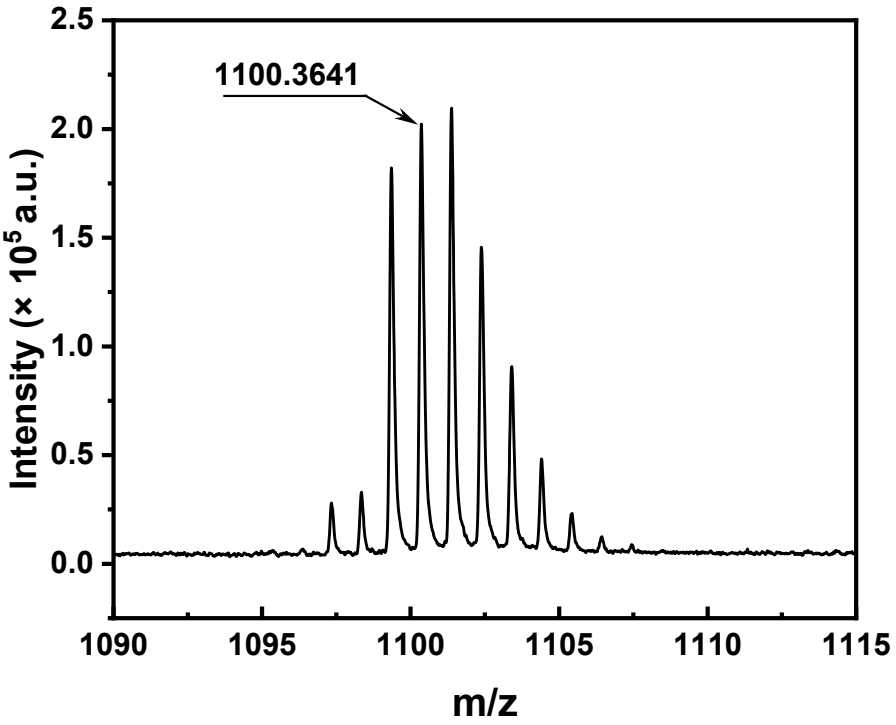

Figure S4. The mass spectroscopy spectrum of F6-IND.

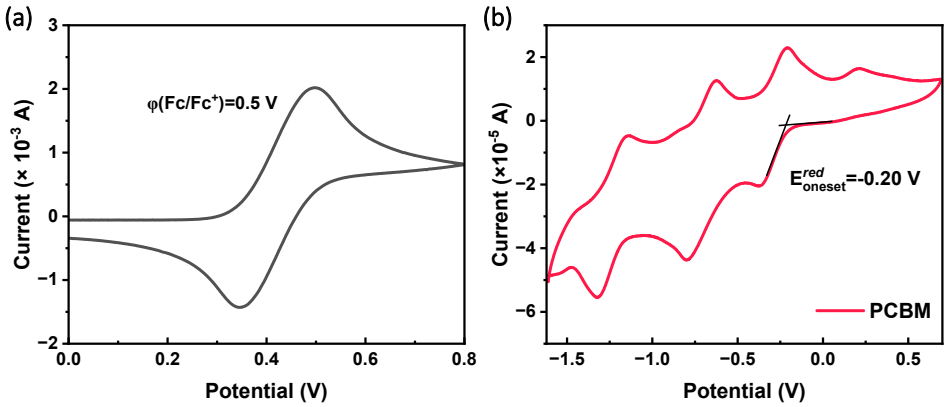

Figure S5. (a) Cyclic voltammograms of Ferrocene in CH_3CN containing 0.1 M *n*-Bu_4NPF_6; (b) Cyclic voltammograms of Ferrocene of PCBM in *o*-DCB/CH_3CN mixed solvent (5:1, v/v) containing 0.1 M *n*-Bu_4NPF_6.

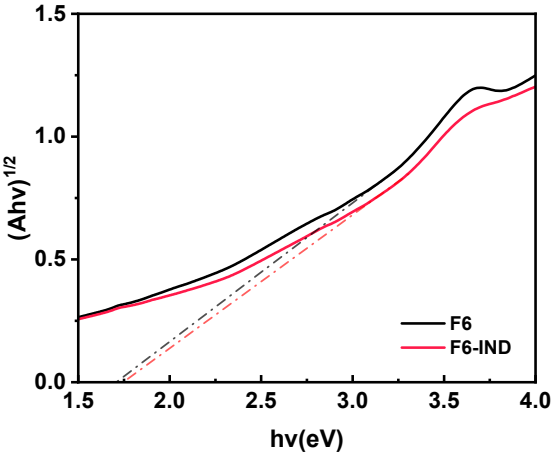

Figure S6. Tauc plots with an estimated optical band gaps are 1.70 eV for F6 and 1.74 eV for F6-IND.

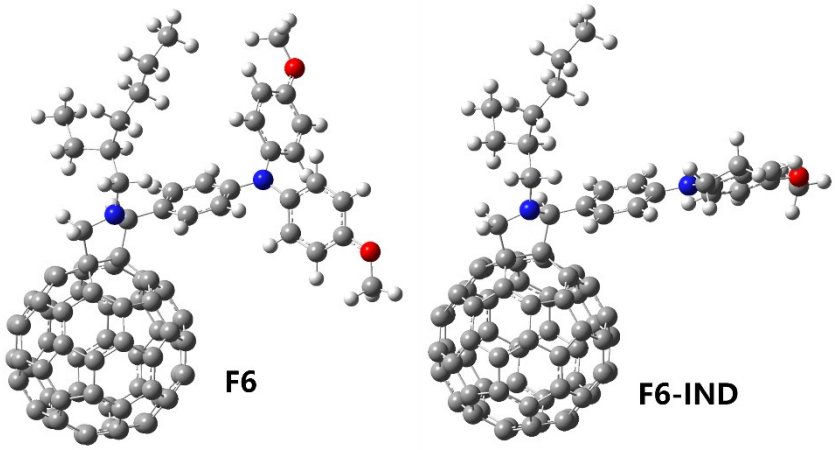

Figure S7. Optimized molecular geometries of F6 and F6-IND obtained from DFT calculations.

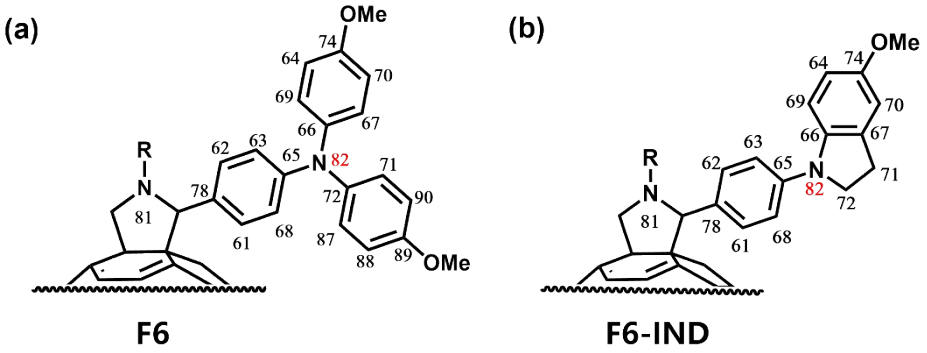

Figure S8. Atomic numbering schemes for (a) F6 and (b) F6-IND.

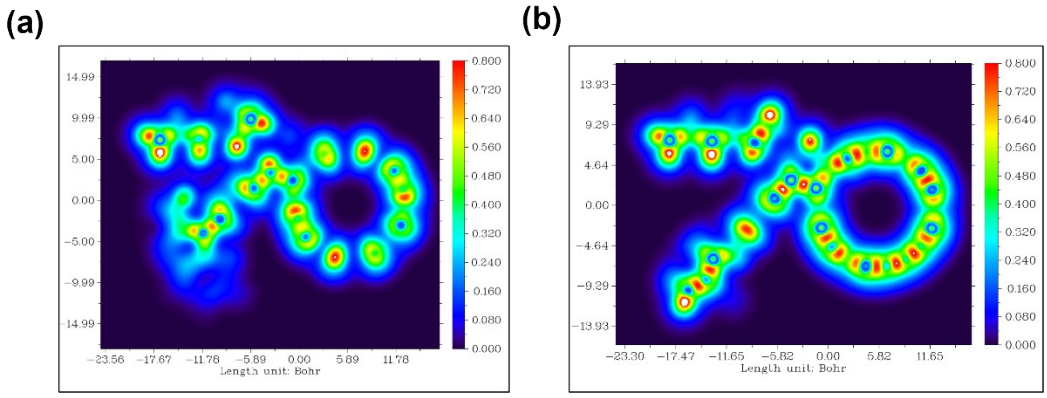

Figure S9. Localized Orbital Locator (LOL) iso surfaces for F6 (a) and F6-IND (b).

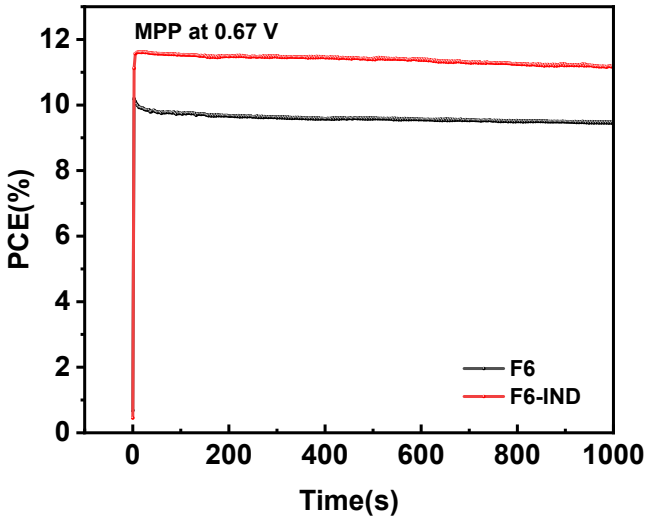

Figure S10. Steady-state power output measured at the maximum power point (MPP) for F6 and F6-IND device

Table S1. Summary of optical and electrochemical properties of F6 and F6-IND.

	HOMO[a] (eV)	LUMO[a] (eV)	$E_{g\ opt}$ (eV)	HOMO[b] (eV)	LUMO (eV)	μ_e ($\times 10^{-4}$ cm^{-2} V^{-1} s^{-1})
F6	-4.38	-2.97	1.70	-5.75	-4.05	1.72
F6-IND	-4.99	-3.05	1.74	-5.70	-3.96	2.23

[a] Calculated from DFT. [b] Determined from $E_{HOMO} = E_{LUMO} - E_g$.

Table S2. Natural bond orbital (NBO) summary for the the triphenylamine donor nitrogen (N82) lone pair in F6 and indoline donor nitrogen (N82) long pair in F6-IND.

	NBO Type	Occupancy (e^-)	Energy (a.u.)	Principal Delocalizations (geminal, vicinal, remote)
F6	LP (1) N 82	1.72606	-0.23293	1413(v), 1438(v), 1423(v), 1421(v), 1422(v), 1437(v), 1432(v), 947(v), 1419(v), 1412(v), 1017(v), 957(v), 1018(v), 958(v)
F6-IND	LP (1) N 82	1.69563	-0.23763	1338(v), 1328(v), 1352(v), 926(v), 1351(v), 936(v), 1334(v), 1327(v), 1347(v), 997(v)

Table S3. Second-Order Perturbation Analysis for the Lone Pair on N82 in F6-IND.

Acceptor NBO (j)	Type	Atoms Involved	E(2) (kcal mol^{-1})	ΔE (a.u.)	F(i,j) (a.u.)
RY*(3) C65	Rydberg	—	2.59	1.76	0.065
RY*(3) C66	Rydberg	—	2.19	1.80	0.061
RY*(4) C72	Rydberg	—	0.64	1.88	0.033
BD*(1) C63–C65	σ*	C63–C65	1.17	0.80	0.029
BD*(2) C63–C65	**π***	**C63–C65**	**34.45**	**0.27**	**0.089**
BD*(1) C65–C68	σ*	C65–C68	1.59	0.80	0.034
BD*(1) C66–C69	σ*	C66–C69	0.50	0.83	0.020
BD*(2) C66–C69	**π***	**C66–C69**	**36.46**	**0.28**	**0.092**
BD*(1) C71–C72	σ*	C71–C72	0.72	0.60	0.020
BD*(1) C72–H97	σ*	C72–H97	2.36	0.69	0.039
BD*(1) C72–H98	σ*	C72–H98	6.46	0.67	0.063

Table S4. Second-Order Perturbation Analysis for the Lone Pair on N82 in F6.

Acceptor NBO (j)	Type	Atoms Involved	E(2) (kcal mol⁻¹)	ΔE (a.u.)	F(i,j) (a.u.)
RY*(3) C65	Rydberg	—	2.12	1.86	0.060
RY*(3) C66	Rydberg	—	1.40	1.23	0.040
RY*(4) C66	Rydberg	—	0.65	2.04	0.035
RY*(3) C72	Rydberg	—	1.54	1.27	0.042
RY*(4) C72	Rydberg	—	0.67	2.13	0.036
BD*(1) C63–C65	σ*	C63–C65	2.02	0.80	0.038
BD*(2) C63–C65	**π***	**C63–C65**	**28.10**	**0.27**	**0.080**
BD*(1) C65–C68	σ*	C65–C68	2.05	0.80	0.039
BD*(1) C66–C67	σ*	C66–C67	4.00	0.80	0.054
BD*(1) C66–C69	σ*	C66–C69	3.72	0.81	0.052
BD*(2) C66–C69	**π***	**C66–C69**	**14.78**	**0.27**	**0.058**
BD*(1) C71–C72	σ*	C71–C72	3.62	0.80	0.051
BD*(1) C72–C87	σ*	C72–C87	3.64	0.81	0.052
BD*(2) C72–C87	π*	**C72–C87**	15.89	0.27	0.060

Table S5. Natural Population Analysis for N82 in F6 and F6-IND.

	Atom	Charge	Core	Valence	Rydberg	Tota
F6	N 82	-0.446	1.999	5.433	0.015	7.446
F6-IND	N 82	-0.427	1.999	5.416	0.012	7.427

Table S6. Detailed photovoltaic parameters for n-i-p TPSCs (**Forward scan)**.

ETLs		V_{oc} (mV)	J_{sc} (mA cm^{-2})	FF (%)	PCE (%)
F6-IND	Best	794	21.80	72.4	12.54
	Avg.	800±20.09	20.87±0.60	68.7±2.23	11.48±0.46
F6	Best	726	21.36	65.8	10.21
	Avg.	724±21.45	20.49±0.60	65.2±1.76	9.68±0.28
PCBM	Best	651	21.84	67.6	9.61
	Avg.	649±7.84	21.04±0.87	65.7±2.82	8.98±0.40

Table S7. TRPL decay fitting parameters of F6 and F6-IND coated perovskite film.

	A_1 (%)	τ_1 (ns)	A_2 (%)	τ_2 (ns)	τ_{avg} (ns)

F6	87.1	14.8	12.9	23.5	16.4
F6-IND	96.6	7.5	3.4	13.6	7.8

Table S8. EIS parameters derived from the equivalent circuit fitting for different devices.

	R_s(Ω)	R_{rec}(kΩ)
F6	4.23	0.95
F6-IND	3.91	2.49

Table S9. Summary of LUMO energy shifts in fullerene derivatives with different structural modifications.

Strategy	Example System	Modification Type	ΔLUMO (meV)	Ref.
Decreasing the size of fullerene π-systems	56π-electron conjugated system	bis-addition PCBM vs bis-PCBM	100	[7]
	56π-electron conjugated system	bis-addition ICBA vs ICMA	120	[8]
Changing the shape of fullerene π-systems	58π-electron conjugated system	1,2-additon SIMEF vs PCBM	100	[9]
	56π-electron conjugated system	regio-isomer *trans*-2 vs *trans*-3	170	[10]
Installation of Electron-donating group	58π-electron conjugated system	methoxy substitution 2,4,6-OMe- vs PCBM	30	[11]
	58π-electron conjugated system	introduction tri-thiophene F3 vs F1	40	[12]
	58π-electron conjugated system	introduction phenyls F2 vs F5	60	[13]
	58π-electron conjugated system	indoline substitution F6-IND vs F6	90	This work

Reference

[1] T. Nakamura, T. Nagai, Y. Miyake, T. Yamada, M. Miura, H. Yoshida, Y. Kanemitsu, M. A. Truong, R. Murdey, A. Wakamiya, *Chem. Sci.* **2025**, *16*, 2265.

[2] A. S. D. Sandanayaka, K. Matsukawa, T. Ishi-i, S. Mataka, Y. Araki, O. Ito, *J. Phys. Chem. B* **2004**, *108*, 19995.

[3] Y. Zou, J. Liu, Y. Chang, C. Duan, W. Han, W. Zhan, Y. Liang, J. Guo, H. Wang, Y. Liao, F. Liu, S. Wang, B. Li, Y. Miao, Y. Chen, Y. Wang, Y. Wang, Y. Zhao, *Adv. Mater.* **2026**, *38*, e22717.

[4] L. Yuan, W. Zhu, Y. Zhang, Y. Li, C. C. S. Chan, M. Qin, J. Qiu, K. Zhang, J. Huang, J. Wang, H. Luo, Z. Zhang, R. Chen, W. Liang, Q. Wei, K. S. Wong, X. Lu, N. Li, C. J. Brabec, L. Ding, K. Yan, *Energy Environ. Sci.* **2023**, *16*, 1597.

[5] T. Lu, F. Chen, *J. Comput. Chem.* **2012**, *33*, 580.

[6] C. Wu, W. Zhu, S. Wang, Z. Cao, L. Ding, F. Hao, *Chem. Commun.* **2022**, *58*, 13007.

[7] M. Lenes, G.-J. A. H. Wetzelaer, F. B. Kooistra, S. C. Veenstra, J. C. Hummelen, P. W. M. Blom, *Adv. Mater.* **2008**, *20*, 2116.

[8] Y. He, H.-Y. Chen, J. Hou, Y. Li, *J. Am. Chem. Soc.* **2010**, *132*, 1377.

[9] Y. Matsuo, Y. Sato, T. Niinomi, I. Soga, H. Tanaka, E. Nakamura, *J. Am. Chem. Soc.* **2009**, *131*, 16048.

[10] C. Sun, P. Yang, Z. Nan, C. Tian, Y. Cai, J. Chen, F. Qi, H. Tian, L. Xie, L. Meng, Z. Wei, *Adv. Mater.* **2023**, *35*, 2205603.

[11] F. B. Kooistra, J. Knol, F. Kastenberg, L. M. Popescu, W. J. H. Verhees, J. M. Kroon, J. C. Hummelen, *Org. Lett.* **2007**, *9*, 551.

[12] Z. Xing, F. Liu, S.-H. Li, Z.-C. Chen, M.-W. An, S. Zheng, A. K.-Y. Jen, S. Yang, *Adv. Funct. Mater.* **2021**, *31*, 2107695.

[13] A. V. Mumyatov, F. A. Prudnov, L. N. Inasaridze, O. A. Mukhacheva, P. A. Troshin, *J. Mater. Chem. C* **2015**, *3*, 11612.